Food Chemistry 520 (2026) 149840

Contents lists available at ScienceDirect

Food Chemistry

journal homepage: www.elsevier.com/locate/foodchem

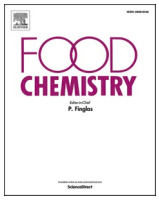

Valorizing banana peel into carbon dots via pyrolysis: CCD optimization and machine learning prediction of fluorescent properties☆

Duyen H.H. Nguyen [a,b,c,*], József Prokisch [a]

[a] Institute of Animal Science, Faculty of Agricultural and Food Sciences and Environmental Management, Biotechnology and Nature Conservation, University of Debrecen, 138 Böszörményi Street, 4032 Debrecen, Hungary
[b] Institute of Life Sciences, Vietnam Academy of Science and Technology, 9/621 Vo Nguyen Giap Street, Linh Trung Ward, Thu Duc City, Ho Chi Minh City, Viet Nam
[c] Doctoral School of Nutrition and Food Science, University of Debrecen, Hungary

ARTICLE INFO

Keywords:
Carbon dots
Carbon Nanodots
Banana peel
Pyrolysis
Central composite design
Random Forest
Machine learning
Fluorescence intensity
Sustainable nanomaterials

ABSTRACT

Carbon dots (CDs) derived from biomass waste represent a sustainable alternative to conventional fluorescent nanomaterials. In this study, highly fluorescent CDs were synthesized from banana peel by pyrolysis using an integrated approach combining Central Composite Design (CCD) and machine learning (ML). The workflow included precursor screening, CCD-based optimization, ML prediction of fluorescence intensity, and environmental stability evaluation. Among the tested precursors, urea was the most effective for enhancing fluorescence performance and quantum yield. CCD identified the key synthesis parameters affecting fluorescence, and the optimized conditions yielded a predicted fluorescence intensity of 16,696 a.u., with quantum yield approaching 40%. Among seven ML algorithms, Random Forest showed the best overall predictive performance, achieving the highest cross-validated R^2 of 0.97 with a low RMSE of 542.14. Feature importance analysis revealed that measured carbon content (C0) was the dominant predictor when elemental descriptors were included, while the precursor-to-banana-peel mass ratio (m_P2) was the most important controllable synthesis factor. Urea-derived BP-CDs retained approximately 97% fluorescence intensity at 1.0 M NaCl and maintained stable emission across pH 3–11. These findings demonstrate a data-guided strategy for producing high-performance, environmentally robust CDs from agricultural waste.

1. Introduction

The growing demand for sustainable nanomaterials has intensified research into carbon dots (CDs), a class of fluorescent carbon-based nanoparticles (<10 nm) valued for their tunable photoluminescence, biocompatibility, low toxicity, and rich surface functionality (Nguyen, El-Ramady, & Prokisch, 2024; Xu et al., 2004). These properties have enabled their widespread use in bioimaging, chemical sensing, optoelectronics, catalysis, and drug delivery, making CDs attractive alternatives to traditional semiconductor quantum dots because of their lower toxicity, better environmental compatibility, and easier processability (Hui et al., 2019; Li et al., 2012; M. Liu, 2020; D. H. H. Nguyen et al., 2025). Among various synthetic approaches, biomass-derived CDs have emerged as particularly promising due to their low cost, environmental compatibility, and alignment with circular economy principles (Bosu et al., 2023; Jamaludin et al., 2019; D. Nguyen, Muthu, et al., 2024).

Banana peel waste represents a valuable and underutilized biomass feedstock for CDs synthesis. With global banana production exceeding 114 million tons annually, peel waste accounts for approximately 40% of total biomass, contributing to significant organic waste (Yasin et al., 2025). Valorizing banana peel into high-performance nanomaterials presents dual benefits: reducing environmental burden and generating economic value (Boyle et al., 2025). Chemically, banana peels are rich in cellulose, hemicellulose, lignin, and heteroatoms (notably nitrogen and oxygen), with reported values of 9.90%, 41.38%, and 8.90%, respectively, which favor carbonization and heteroatom doping under thermal treatment (Kabenge et al., 2018). Doping CDs with different precursors is a well-known strategy for significantly influencing the quantum yield and emission characteristics of CDs (W. Liu et al., 2017; J. Wang et al.,

☆ This article is part of a Special issue entitled: '4th Food Chemistry Conference' published in Food Chemistry.

* Corresponding authors at: Institute of Animal Science, Faculty of Agricultural and Food Sciences and Environmental Management, Biotechnology and Nature Conservation, University of Debrecen, 138 Böszörményi Street, 4032 Debrecen, Hungary.
E-mail address: nguyen.huu.huong.duyen@agr.unideb.hu (D.H.H. Nguyen).

https://doi.org/10.1016/j.foodchem.2026.149840
Received 23 March 2026; Received in revised form 19 May 2026; Accepted 26 May 2026
Available online 28 May 2026

2015). Therefore, banana peel is not only an abundant waste material but also a chemically suitable precursor for developing fluorescent carbon nanomaterials.

Pyrolysis offers a scalable and simple method for synthesizing CDs from banana peel, allowing control over doping and surface functionalization (Kostromin et al., 2023; Stan et al., 2015). However, the optical properties and performance of CDs are strongly dependent on synthesis conditions, such as temperature (Santos et al., 2025), duration, and precursor ratios (Ogi et al., 2016). Traditional optimization methods, particularly one-factor-at-a-time (OFAT) approaches, are inefficient and overlook critical interactions among variables. To overcome these limitations, statistical design of experiments techniques such as Response Surface Methodology (RSM), particularly Central Composite Design (CCD), have been increasingly applied to explore multivariable parameter spaces while minimizing experimental runs systematically (Gilman et al., 2021). Nevertheless, the use of CCD in biomass-derived CD systems remains limited, especially for systematically analyzing the combined effects of precursor ratio, pyrolysis temperature, and reaction time on fluorescence performance.

Machine learning (ML) has emerged as a powerful tool in nanomaterials research, offering predictive capabilities for synthesis-property relationships and accelerating material discovery (Diao et al., 2025). In recent studies, ML has been applied to model complex and nonlinear relationships between processing variables and material properties, predict performance from experimental descriptors, and support reaction optimization in nanomaterial systems (Dr Sheela Hundekari et al., 2024; Gao et al., 2025). Algorithms such as Random Forest (RF), Decision Trees (DT), Support Vector Regression (SVR), and Artificial Neural Networks (ANN) are particularly useful because they can capture multivariate interactions that are difficult to resolve using conventional statistical approaches alone (Chakravarthi et al., 2024). For carbon-based nanomaterials, such data-driven methods are especially relevant because fluorescence behavior is governed by multiple interdependent factors, including precursor composition, temperature, time, and surface chemistry (Han et al., 2020; Senanayake et al., 2022). However, ML applications remain largely unexplored in the context of banana peel-derived CDs, particularly for integrating synthesis optimization and property prediction.

Despite the progress in biomass-derived CDs research, several important gaps remain. First, comparative studies on different added precursors for banana peel-based CDs are still limited, making it difficult to identify the most effective precursor for improving fluorescence properties. Second, the interactive effects among key pyrolysis parameters are not yet sufficiently understood, although these interactions are essential for tuning fluorescence intensity. Third, the integration of ML with experimental optimization has not been adequately explored for banana peel-derived CDs, limiting the development of predictive and transferable synthesis frameworks.

To address these deficiencies, this study proposes a sequential and integrated strategy. First, different precursors were screened to identify their influence on the fluorescence performance of banana peel-derived CDs. Second, a face-centered CCD was applied to optimize pyrolysis temperature (160–200 °C), time (1–4 h), and urea-to-banana peel mass ratio (4:1 to 4:3), thereby enabling systematic evaluation of both individual and interaction effects. Finally, several ML models were developed and compared to identify the most suitable model for predicting fluorescence intensity from synthesis variables. Through this approach, the present work not only identifies effective synthesis conditions for high-performance BP-CDs but also establishes a data-driven framework for sustainable nanomaterial production from agricultural waste. This work contributes a scalable, data-driven approach to sustainable nanomaterial production and highlights the potential of banana peel valorization for high-performance CD synthesis.

2. Materials and methods

2.1. Materials

Fresh banana peels from *Musa acuminata* (Cavendish cultivar, origin: Panama) were obtained from Dr. Aliment Company (Debrecen, Hungary). The peels were thoroughly washed with distilled water, freeze-dried, and ground into a fine powder for use as the carbon source. Food-grade chemical precursors, including urea, citric acid, glycine, and dextrose, were purchased from commercial suppliers and used without further purification. All experiments utilized ultrapure water. All synthesis and characterization experiments were performed in triplicate.

2.2. Equipments

Instrumentation employed for sample analysis and characterization included a Lambda 35 UV–Vis spectrophotometer (PerkinElmer Inc., Norwalk, USA), an FP-8500 fluorescence spectrophotometer (Jasco Co., Oklahoma, USA), a 4300 Handheld FTIR spectrometer (Agilent Technologies, California, USA), and a JEM-2000FXII transmission electron microscope (JEOL Ltd., Tokyo, Japan). High-performance liquid chromatography (HPLC) analysis was conducted using the ECS05 Gradient Analytical HPLC System (ECOM Co., Praha, Czech Republic) equipped with a Nucleosil C18 100 Å column (5 µm, 150 × 4.6 mm, Phenomenex Corp., California, USA) and a UV–VIS PDA detector (ECDA2800, ECOM Co.). Additional purification of CDs was performed using an ECOM ECB2000 HPLC system coupled with an RF-20 A XS fluorescence detector (Shimadzu Co., Kyoto, Japan) and a BioSep-SEC-S 2000 column (60 × 21.20 mm, Phenomenex, California, USA).

To contextualize the relevance of banana peels as a raw material, Table 1 summarizes their proximate composition as reported in the literature (Yasin et al., 2025).

2.3. Experimental design

The experimental workflow used to optimize the synthesis of banana peel-derived carbon dots (BP-CDs) is presented in Fig. 1. Initially, banana peel (BP) was combined with four precursor groups, namely urea, citric acid, glycine, and sugars, and the resulting mixtures were subjected to pyrolysis at 180 °C for 1–4 h. The precursor system yielding BP-CDs with the highest fluorescence intensity was selected for subsequent optimization. Based on this screening step, the BP–urea system was identified as the most promising formulation.

Optimization of the selected system was then performed using a central composite design (CCD). In this stage, the precursor type was fixed as P_2_Urea, and three independent variables were investigated: the mass ratio between BP and urea (m_P2), pyrolysis time, and pyrolysis temperature. The CCD was used to systematically evaluate the individual and interactive effects of these three factors on the fluorescence intensity of BP-CDs and to determine the synthesis conditions associated

Table 1
Banana peel composition from the literature (Yasin et al., 2025).

Components	Composition Range
Moisture	4.6–95%
Carbohydrates	11.8–68.3%
Potassium	4.39–2244.7 mg/100 g
Magnesium	29.4–710 mg/100 g
Calcium	41–440 mg/100 g
Sodium	11.6–180 mg/100 g
Phosphorus	27.8–211.3 mg/100 g
Crude Fiber	4.2–16.6%
Crude Protein	1.9–13.4%
Crude Fat	1.2–7.6%
Trace elements	Iron: 0.07–47.0 *mg/100 g* Zinc: 0.033–0.41 *mg/100 g* Copper: 0.15–0.51 *mg/100 g*

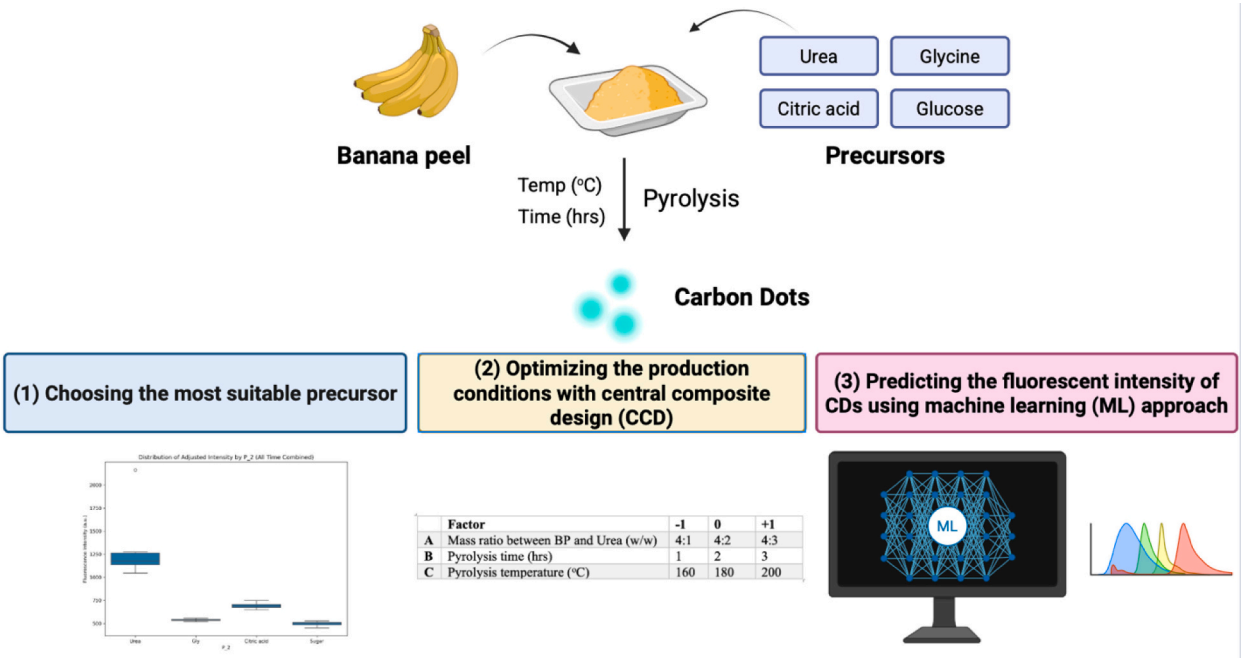

	Factor	-1	0	+1
A	Mass ratio between BP and Urea (w/w)	4:1	4:2	4:3
B	Pyrolysis time (hrs)	1	2	3
C	Pyrolysis temperature (°C)	160	180	200

Fig. 1. Schematic diagram of a three-stage experimental design to optimize the production conditions of carbon dots from banana peel (BP-CDs) using central composite design (CCD) and machine learning (ML) approach.

with the highest response.

The experimental data obtained from both the precursor screening and CCD optimization were further used to develop machine learning (ML) models for fluorescence prediction. A total of 396 data points were included in the dataset, of which 80% were allocated to the training set and 20% to the test set. To improve model robustness and reduce the risk of overfitting, 5-fold cross-validation was applied during the training process. In addition, hyperparameter tuning was performed for all seven evaluated models using GridSearchCV on the training set only. The tested models included Linear Regression, K-Nearest Neighbors, Support Vector Regression, Decision Tree, Random Forest, Gradient Boosting, and Artificial Neural Network (MLPRegressor). For each model, the best hyperparameter combination was selected based on cross-validated predictive performance before final evaluation on the independent test set. In contrast to the CCD analysis, which was limited to the three synthesis variables within the fixed BP–urea system, the ML analysis incorporated all available factors relevant to fluorescence prediction, including precursor type, carbon content (%C), nitrogen content (%N), BP-to-precursor mass ratio (m_P2), pyrolysis time, and pyrolysis temperature.

Model performance was assessed using the coefficient of determination (R^2) and root mean square error (RMSE). The model showing the best predictive performance was selected as the final model and used as a data-driven tool to estimate the fluorescence intensity of BP-CDs from compositional and process-related variables, thereby supporting the optimization of synthesis conditions.

2.3.1. Synthesis of carbon dots from banana peel (BP-CDs) via pyrolysis

Banana peel powder was mixed with precursors at a mass ratio 4:1 (*w*/w) and subjected to pyrolysis in an oven at a temperature of 200 °C for 3 h. Two reference samples were prepared in parallel for comparative analyses: (i) a pre-pyrolysis mixture of banana peel and each precursor, sampled before heat treatment and used as the baseline for elemental composition analysis (Fig. 3**F** and **G**); and (ii) a no-precursor BP-CDs sample, prepared by pyrolyzing banana peel alone under the same conditions and used as a benchmark for the precursor-screening comparison (Fig. 3C, D, and E).The obtained samples were mixed with ultrapure water in the ratio of 1:10 (w/w) and subjected to ultrasound for 30 min for extraction. The isolated CDs solution was collected by filtering the sample with a 0.22 μm filter paper. BP-CDs were isolated by preparative size-exclusion HPLC with fluorescence detection (HPLC-SEC-FD) following the method previously developed and validated by our group (Prokisch et al., 2026). Separation was performed on a BioSep-SEC-S 2000 column (60 × 21.20 mm, Phenomenex) using an ECOM ECB2000 system coupled with a Shimadzu RF-20 A XS fluorescence detector (λ_ex/λ_em = 360/450 nm) under isocratic conditions with deionized water as the mobile phase (flow rate 0.7 mL/min; injection volume 5 μL). Based on the SEC calibration established in our previous study, fluorescence-active peaks eluting before ~10 min correspond to nanoparticle-sized species (approximate molecular weight 200–1000 kDa, equivalent to particle sizes of several nanometers), whereas later-eluting peaks correspond to smaller fluorescent molecular fragments (Prokisch et al., 2026). The synthesized BP-CDs were characterized by UV–Vis absorption spectroscopy, fluorescence spectroscopy, quantum yield measurements, TEM and HPLC-SEC-FD (Fig. 2**)**.

2.3.2. Quantum yield measurement

The quantum yield (QY) of the carbon nanodots was determined using a comparative method with quinine sulfate (QY = 0.54 in 0.1 M H_2SO_4) as the reference standard. Briefly, both the sample and standard solutions were prepared to ensure absorbance values below 0.1 at the excitation wavelength (typically 360 nm) to minimize reabsorption effects. The fluorescence emission spectra were recorded using a FP-8500 fluorescence spectrophotometer under identical instrumental settings.

Before QY calculation, each emission spectrum was blank-corrected by subtracting the corresponding solvent blank recorded under the same conditions: deionized water for BP-CDs and 0.1 M H_2SO_4 for quinine sulfate. The integrated fluorescence intensities were obtained by numerical integration of the emission spectra over 380–700 nm, covering the full emission bands of both the samples and reference. The QY was calculated using the following equation:

$$\Phi_s = \Phi_r \left(\frac{I_s}{I_r}\right)\left(\frac{A_r}{A_s}\right)\left(\frac{n_s^2}{n_r^2}\right)$$

where:

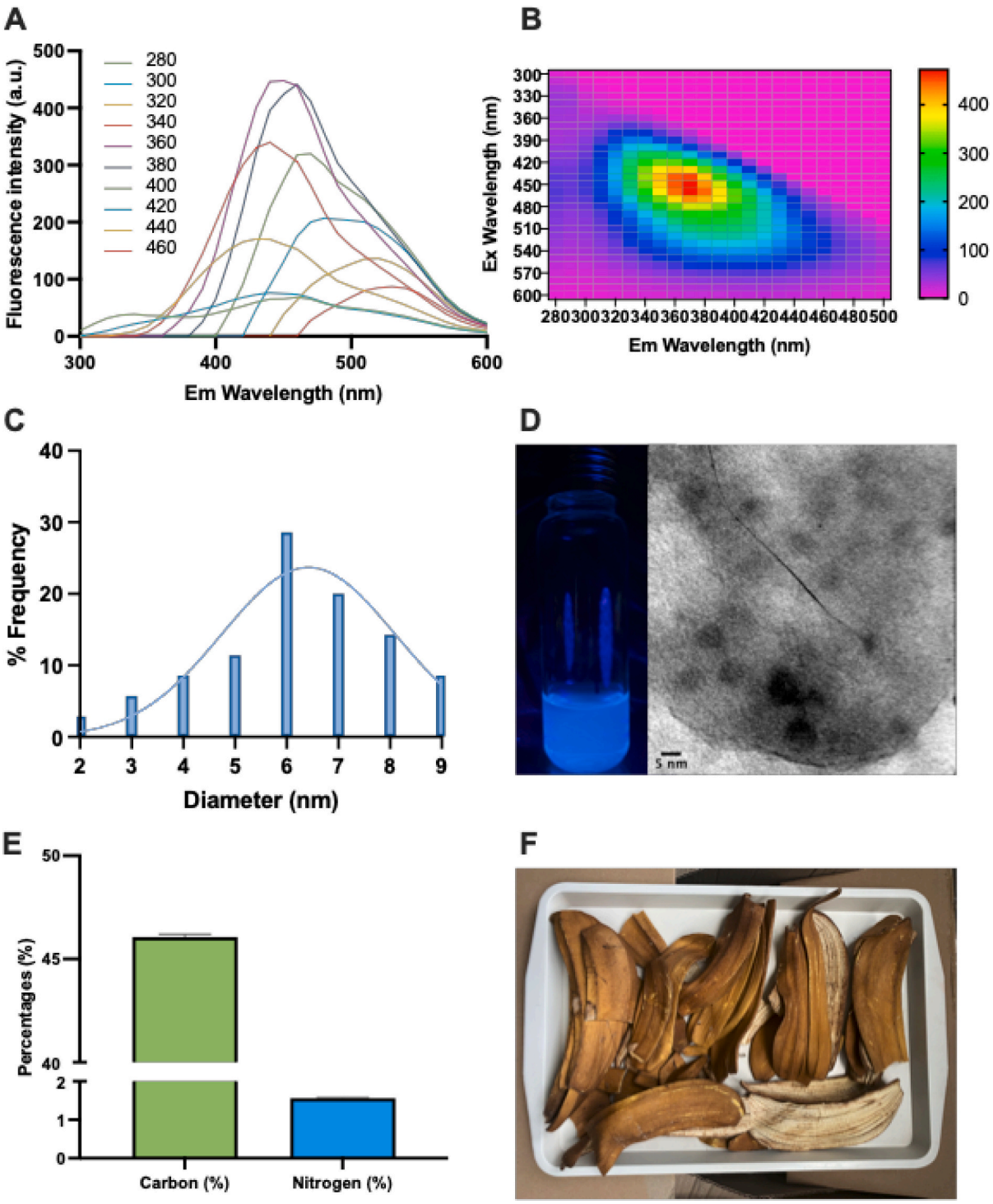

Fig. 2. Evaluation of fluorescence and elemental composition of freeze-dried banana peel (BP) for carbon dots synthesis. (**A**) Fluorescence emission spectra of BP extract at various excitation wavelengths. The strongest fluorescence intensity was observed at 360 nm, which was selected for subsequent measurements. (**B**) Excitation-emission matrix (EEM) plot of BP extract, illustrating fluorescence behavior across different excitation/emission combinations. (**C**) Size distribution histogram of CDs synthesized from BP (BP-CDs). (**D**) Left: Visual fluorescence of BP extract under UV light. Right: Transmission electron microscopy (TEM) image of BP-CDs showing an average size of 6.42 ± 1.67 nm. (**E**) Elemental composition of freeze-dried BP, showing carbon and nitrogen content (%) relevant to carbonization and in-situ nitrogen doping. (**F**) Photograph of freeze-dried banana peel samples, showing their typical physical appearance and uniform preservation quality.

- Φ_s and Φ_r are the quantum yields of the sample and reference, respectively,
- I_s and I_r are the integrated fluorescence intensities,
- A_s and A_r are the absorbances at the excitation wavelength,
- n_s and n_r are the refractive indices of the solvents used for the sample and reference, respectively.

The refractive indices used were 1.333 for water and 1.334 for 0.1 M H_2SO_4. Since both systems were dilute aqueous solutions, the refractive index correction was close to unity. All measurements were performed at room temperature, and each experiment was repeated in triplicate to ensure reproducibility.

2.3.3. Central composite design to optimum pyrolysis conditions to produce BP-CDs

Following precursor selection, a Central Composite Design (CCD) was employed to optimize the synthesis conditions for banana peel-derived carbon dots (BP-CDs). The CCD model was used to investigate the effects of three independent variables: (A) mass ratio between banana peel and urea (*w*/w), (B) pyrolysis time (h), and (C) pyrolysis temperature (°C). Each variable was evaluated at three coded levels (−1, 0, +1), as shown in Table 2.

The CCD matrix consisted of factorial, axial, and center points, allowing the estimation of both linear and quadratic effects, as well as interaction terms. This design enabled an efficient exploration of the synthesis space using a minimal number of experimental runs. The full experimental matrix with coded and actual levels for each condition is presented in Table 3.

The response variable was the fluorescence intensity of the synthesized CDs. A second-order polynomial regression model was used to fit the data:

$$Y = \beta_0 + \Sigma\beta_i X_i + \Sigma\beta_{ii} X_i^2 + \Sigma\beta_{ij} X_i X_j$$

where Y is the predicted fluorescence intensity, X_i and X_j are the coded variables, and β_0, β_i, β_{ii}, and β_{ij} are the regression coefficients for the intercept, linear, quadratic, and interaction effects, respectively.

2.3.4. Machine learning model development

A dataset of synthesis parameters and corresponding fluorescence intensities was used to train ML models, including Random Forest, Support Vector Regression, Artificial Neural Networks, Gradient Boosting, Decision Tree, Linear Regression, and K-Neighbors Regression. Model performance was evaluated by R^2, and RMSE was used to evaluate model performance. The best-performing model was then applied to predict fluorescence intensity from synthesis conditions, enabling efficient, data-driven optimization.

2.3.5. Stability evaluation of BP-CDs

2.3.5.1. Ionic-strength (NaCl) stability. The fluorescence stability of BP-CDs under varying ionic strengths was evaluated by measuring fluorescence intensity in NaCl solutions of 0, 0.1, 0.2, 0.3, 0.4, 0.5, 0.6, 0.7, 0.8, 0.9, and 1.0 M. For each measurement, an aliquot of the CDs solution was diluted 8-fold with the corresponding NaCl solution, mixed gently, and equilibrated at room temperature for 10 min before measurement. Five samples were evaluated: (S1) banana peel extract before pyrolysis, (S2) no-precursor BP-CDs (banana peel pyrolyzed alone), (S3) citric-acid-BP-CDs, (S4) urea-BP-CDs, and (S5) glycine-BP-CDs.

2.3.5.2. pH stability. The fluorescence stability of the three precursor-derived BP-CDs (S3, S4, and S5) was further evaluated across pH 3, 5, 7, 9, and 11. Universal Britton–Robinson buffer was prepared by titrating a mixture of 0.04 M phosphoric, acetic, and boric acids with 0.2 M NaOH to the target pH. For each measurement, CDs samples were diluted 8-fold with the corresponding buffer and equilibrated at room temperature for 10 min before measurement.

For both tests, fluorescence emission spectra were recorded on the FP-8500 fluorescence spectrophotometer at λ_ex = 360 nm, and peak emission intensity at λ_em ≈ 450 nm was reported. All measurements were performed in triplicate (n = 3 independent samples). Reported intensities were corrected for the 8-fold dilution factor. For NaCl stability, relative fluorescence intensity was additionally calculated as I(NaCl)/I(0 M) × 100%. Statistical significance among NaCl concentrations and pH levels for each sample was assessed by one-way ANOVA followed by Duncan's post hoc test ($p < 0.05$).

Table 2
Independent variables and their coded levels used in CCD for optimizing BP-CDs synthesis.

	Factor	−1	0	+1
A	Mass ratio between BP and Urea (w/w)	4:1	4:2	4:3
B	Pyrolysis time (h)	1	2	3
C	Pyrolysis temperature (°C)	160	180	200

Table 3
Experimental CCD matrix for optimization of BP-CD synthesis.

Run	A_coded	B_coded	C_coded	Ratio (A)	Time (B)	Temp (C)
1	−1	−1	−1	4:1	1	160
2	−1	−1	0	4:1	1	180
3	−1	−1	+1	4:1	1	200
4	−1	0	−1	4:1	2	160
5	−1	0	0	4:1	2	180
6	−1	0	+1	4:1	2	200
7	−1	+1	−1	4:1	3	160
8	−1	+1	0	4:1	3	180
9	−1	+1	+1	4:1	3	200
10	0	−1	−1	4:2	1	160
11	0	−1	0	4:2	1	180
12	0	−1	+1	4:2	1	200
13	0	0	−1	4:2	2	160
14	0	0	0	4:2	2	180
15	0	0	+1	4:2	2	200
16	0	+1	−1	4:2	3	160
17	0	+1	0	4:2	3	180
18	0	+1	+1	4:2	3	200
19	+1	−1	−1	4:3	1	160
20	+1	−1	0	4:3	1	180
21	+1	−1	+1	4:3	1	200
22	+1	0	−1	4:3	2	160
23	+1	0	0	4:3	2	180
24	+1	0	+1	4:3	2	200
25	+1	+1	−1	4:3	3	160
26	+1	+1	0	4:3	3	180
27	+1	+1	+1	4:3	3	200

2.4. Data analysis

All experimental data were processed and analyzed using a combination of Python (v3.9), Microsoft Excel (Microsoft 365), and GraphPad Prism (v9.5). Python libraries such as NumPy, pandas, matplotlib, seaborn, and scikit-learn were employed for data wrangling, statistical analysis, machine learning model development, and visualization. GraphPad Prism was used for statistical testing (e.g., ANOVA) and generating contour plots, while Excel was used for initial data cleaning, matrix construction, and response surface formatting. Data visualizations—including emission spectra, correlation matrices, model fitting curves, and feature importance plots—were created using a combination of these tools to ensure consistency and clarity. All statistical comparisons were considered significant at $p < 0.05$.

3. Results and discussion

3.1. Characterization of carbon dots from banana peel (BP-CDs) and freeze-dried banana peel

Fig. 2 summarizes the characterization results of the BP-CDs and the freeze-dried banana peel precursor. Fig. 2A and Fig. 2B show the fluorescence emission spectra of BP-CDs extract at various excitation wavelengths, with the strongest fluorescence intensity observed at 360 nm, which was selected for subsequent measurements. Fig. 2C displays the size distribution histogram of the synthesized BP-CDs, indicating a narrow size range with an average particle size of 6.42 ± 1.67 nm. Fig. 2D includes TEM images of BP-CDs (right) along with the visual fluorescence of BP extract under UV light (left), confirming successful CDs formation as spherical black particles with strong blue fluorescence. The fluorescence color of BP-CDs was predicted to be blue in most cases

(**Fig. SI.02**). Fig. 2E shows the elemental composition of freeze-dried BP, with carbon and nitrogen content confirming its suitability for carbonization and nitrogen doping. Finally, Fig. 2F presents a photograph of the freeze-dried banana peel samples, illustrating their uniform preservation and physical characteristics, ensuring batch consistency prior to synthesis.

3.2. *Screening of adding precursors for synthesizing carbon dots from banana peel (BP-CDs)*

To evaluate the influence of different precursors on the formation and properties of banana peel-derived carbon dots (BP-CDs), banana peel was thermally processed with urea, glycine, citric acid, or sugar at 180 °C for 1–4 h. The fluorescence intensity of the resulting BP-CDs is presented in Fig. 3A. Among all tested precursors, urea consistently

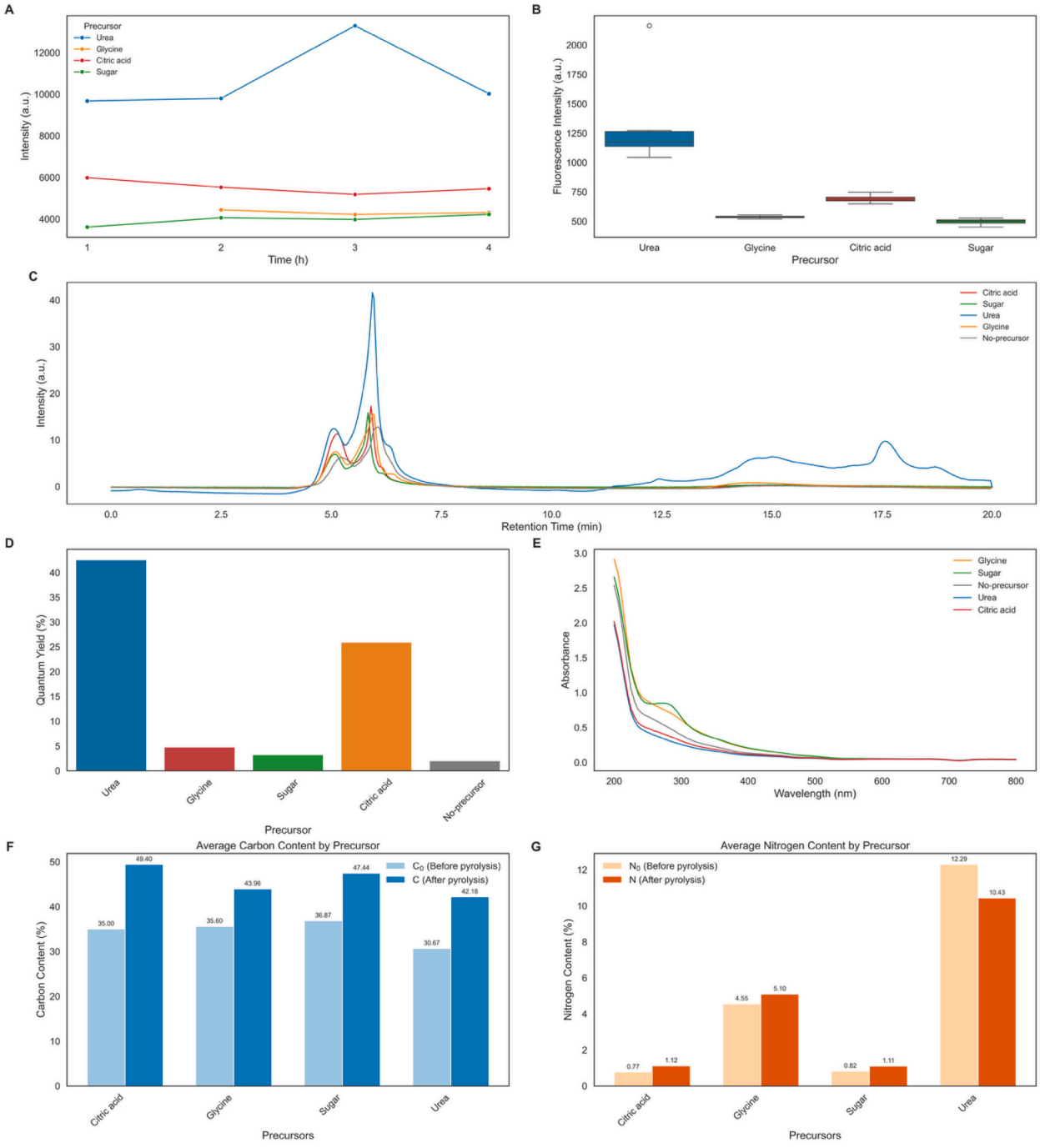

Fig. 3. Effect of different precursors on the fluorescence and physicochemical properties of banana peel-derived carbon dots (BP-CDs). (**A**) Time-dependent fluorescence intensity of BP-CDs synthesized at 180 °C using different precursors (urea, glycine, citric acid, and sugar). (**B**) Box plot of adjusted fluorescence intensity across all time points, grouped by precursor. (**C**) HPLC-SEC-FD chromatograms of BP-CDs prepared with different precursors. The "no-precursor BP-CDs" trace corresponds to banana peel pyrolyzed without an added precursor. (**D**) Quantum yield (%) of BP-CDs. (**E**) UV–Vis absorption spectra of BP-CDs. In all three panels, the no-precursor BP-CDs (banana peel pyrolyzed alone) serves as the reference for the precursor-screening comparison. (**F**) Carbon and (**G**) nitrogen content (%) of BP-CDs prepared with different precursors, comparing the pre-pyrolysis mixtures (C_0 / N_0, before pyrolysis) with the corresponding pyrolyzed samples (C / N, after pyrolysis).

produced the highest fluorescence intensity, reaching a maximum at 3 h. In contrast, glycine, citric acid, and sugar produced substantially lower fluorescence intensities and showed only minor time-dependent changes.

The distribution of fluorescence intensity across all time points (Fig. 3B) further highlights the superior performance of urea. Urea-derived BP-CDs showed a higher median fluorescence intensity and a broader distribution, indicating enhanced emissive properties and greater structural heterogeneity. Elemental analysis further confirmed the influence of precursor type on the elemental composition of BP-CDs (Fig. 3F,G). The urea-derived sample exhibited the highest final nitrogen content (10.55%), followed by the glycine-derived sample (5.06%), whereas the citric acid- and sugar-derived samples showed much lower nitrogen contents of 1.12% and 1.08%, respectively. However, the urea-containing precursor mixture already exhibited a high initial nitrogen content before pyrolysis (12.70%). Therefore, the high final nitrogen content of the urea-derived BP-CDs should be interpreted as reflecting the nitrogen-rich nature of urea and the retention of nitrogen-containing species after pyrolysis, rather than as evidence of higher nitrogen-doping efficiency. Moreover, bulk nitrogen content alone does not fully represent nitrogen-doping efficiency, as the fluorescence behavior of N-doped CDs is more closely associated with the chemical

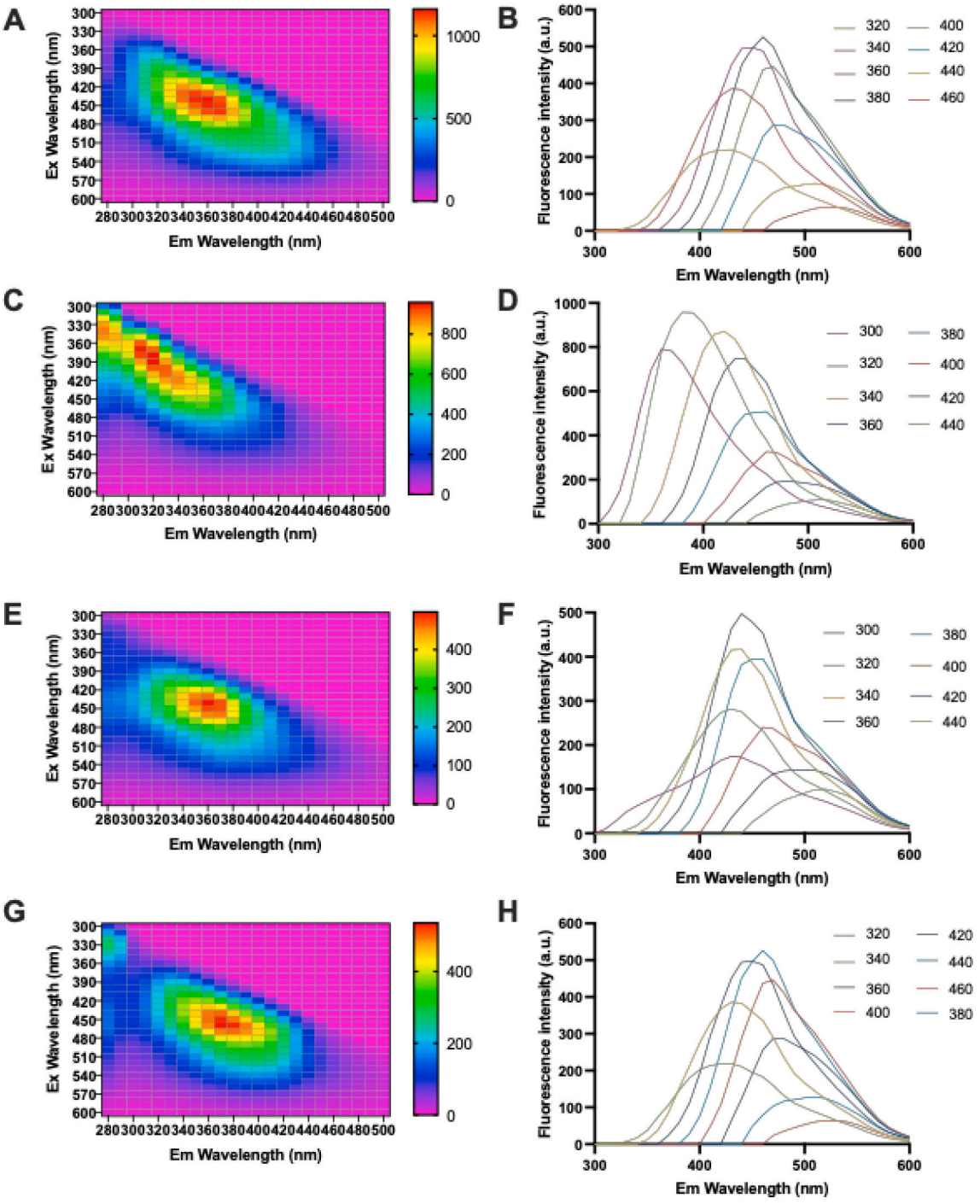

Fig. 4. Excitation-emission matrix plots (left panels) and fluorescence emission spectra at various excitation wavelengths (right panels) of carbon dots synthesized from banana peel (BP-CDs) with different precursors: (**A, B**) Urea-BP-CDs, (**C, D**) Citric Acid-BP-CDs, (**E, F**) Sugar-BP-CDs, (**G, H**) Glycine-BP-CDs.

environment of nitrogen species, including pyridinic, pyrrolic, graphitic, and amino configurations, than with the total nitrogen content alone (Holá et al., 2017; L. Wang et al., 2014). Future studies employing XPS or NMR analysis are therefore required to elucidate nitrogen speciation and its role in fluorescence enhancement.

Although all samples showed increased carbon content after heat treatment, pronounced nitrogen enrichment was observed only in the urea-derived CDs. Chromatographic analysis by HPLC-SEC-FD (Fig. 3C) revealed distinct chemical profiles among the samples. Accordingly, the first fluorescence-active peak (retention time approximately 5–6 min) was assigned to the BP-CDs fraction on the basis of four converging criteria (Prokisch et al., 2026): (i) elution within the nanoparticle MW window previously established for Gly-CSNDs (~800 kDa, ~6.6 nm), consistent with our TEM-measured BP-CDs diameter of 6.42 ± 1.67 nm (Fig. 2D); (ii) strong fluorescence signal at λ_ex/λ_em = 360/450 nm; (iii) a characteristic UV–Vis absorbance pattern in the 230–320 nm region attributable to π–π and n–π* transitions (Fig. 3E); and (iv) elution earlier than the unreacted molecular precursors and smaller fluorescent fragments. The BP-CD fraction was collected manually based on the FD signal threshold, pooled across replicate injections, and used for all downstream characterization.The urea-derived BP-CDs exhibited broader and more intense peaks, including a dominant peak at approximately 6 min, suggesting the formation of higher-molecular-weight and/or more highly conjugated fluorescent species. In contrast, the other precursors produced narrower and less intense peaks, indicating more limited or more homogeneous structures.

To assess optical and quantum efficiency, Fig. 3D presents the quantum yield (QY) of BP-CDs. The urea-derived CDs again showed superior performance, reaching a QY of ~40%, significantly higher than those prepared with glycine, sugar, citric acid, or no precursor BP-CDs. This aligns with the enhanced fluorescence and suggests that nitrogen incorporation may contribute, together with other structural and surface-related changes, to the improved photoluminescent efficiency. Finally, UV–Vis absorption spectra (Fig. 3E) showed broadband absorption in the UV region for all BP-CDs samples. The sugar-derived sample exhibited a more pronounced absorption feature in the 230–280 nm region, which may be attributed to π–π* transitions of sp^2 C═C domains and n–π* transitions of carbonyl or other surface functional groups. Since UV–Vis spectroscopy alone cannot confirm heteroatom doping, this feature was not interpreted as direct evidence of nitrogen doping.

Additional insights were obtained from excitation–emission matrix (EEM) scans and fluorescence emission spectra across a range of excitation wavelengths (Fig. 4). EEM plots revealed that most BP-CDs shared a similar pattern, except for citric acid-BP-CDs (Fig. 4C). All BP-CDs exhibited excitation-dependent emission behavior typical of Urea-BP-CDs (Figs. 4A–B), showing broader and more intense fluorescence domains compared to CDs synthesized using citric acid, sugar, or glycine (Figs. 4C–H). The emission spectra further confirmed the superior brightness and boarder spectra of Urea-BP-CDs, particularly at an excitation wavelength of 360 nm, which produced the highest intensity signal. This optimal excitation wavelength was therefore selected for all subsequent fluorescence measurements and is consistent with our previous work on detecting food-derived CDs (D. Nguyen, Muthu, et al., 2024). In contrast, the CDs from other precursors displayed narrower emission bands with lower overall intensity, supporting the conclusion that urea contributes more effectively to nitrogen incorporation and defect-state formation.

Together, these findings confirm that urea acts as the most effective precursor for improving the optical properties of BP-CDs, leading to enhanced optical properties, chemical complexity, and quantum efficiency. Its superior effect is likely related to its dual role as both a carbon and nitrogen source, promoting efficient nitrogen incorporation during pyrolysis and favoring the formation of emissive surface defects and passivation states. However, this precursor-screening experiment identifies the most effective formulation only at the comparative experimental level; the relative importance of the measured synthesis and compositional variables was evaluated separately by machine learning, as discussed in Section 3.4. This interpretation is consistent with previous studies showing that urea is an effective nitrogen source for improving the fluorescence properties of CDs. For example, (Prado et al., 2023) reported that nitrogen-doped CDs prepared with a 1:6 carbon-to-urea ratio exhibited the highest quantum yield of 19% at pH 11, while (Yorozuya et al., 2025) showed that urea concentration influences both the fluorescence spectra and quantum yield of nitrogen-doped CDs. Furthermore, the optical performance achieved in the present study is comparable to or better than that reported for CDs derived from other biomass sources.

A similar trend is observed when comparing with other biomass-derived CDs reported in the literature. Lemon juice-derived CDs, for example, showed quantum yields ranging from 14.86% to 24.89% depending on hydrothermal temperature (Hoan et al., 2019), while exogenous nitrogen doping in other biomass-based systems has been reported to increase quantum yield from 2.95% to 35.39% (Y. Liu et al., 2022). Additional reports also show substantial variation depending on the biomass source and synthesis strategy. CDs derived from loblolly pine reached a high quantum yield of 48% (Quaid et al., 2022), and zebrafish scale-derived CDs achieved 31.71% (Y. Liu et al., 2024). In contrast, more modest values have been reported for chitosan-derived CDs (15.3%) (Zattar et al., 2021), chia seed-derived CDs (4–25%) (Jones et al., 2017), and banana juice-derived CDs (8.95%)(De & Karak, 2013). These comparisons indicate that the photoluminescent performance of biomass-derived CDs is highly dependent on precursor composition, heteroatom doping, and synthesis conditions. Although direct fluorescence intensity values are difficult to compare across studies because of differences in instruments and measurement conditions, the ~40% quantum yield achieved in the present work is clearly higher than many reported biomass-derived systems and falls within the upper range of currently reported biomass-based CDs. These findings suggest that the optimized BP-CDs prepared here exhibit competitive, and in some cases superior, photoluminescent performance while using a simple and relatively mild synthesis route, highlighting their potential for sustainable and scalable production.

3.3. Optimization of pyrolysis conditions using central composite design (CCD)

A Central Composite Design (CCD) was employed to optimize the synthesis parameters for urea-assisted banana peel-derived carbon dots (U-BP-CDs). The regression model demonstrated a strong fit between predicted and experimental fluorescence intensity values, yielding an R^2 value of 0.886, indicating that approximately 88.6% of the variability in intensity was explained by the model (Fig. 5A). The fitted quadratic regression equation in coded form was:

$$Y = 9057.30 + 4147.28 \times A + 272.20 \times B + 1900.59 \times C + 592.56 \times A2 + 143.28 \times AB + 1456.38 \times AC - 572.51 \times B2 + 892.25 \times BC - 1193.28 \times C2$$

where A, B, and C represent the coded values for mass ratio, reaction time, and temperature, respectively.

The ANOVA results (**Fig. SI.01**) revealed that mass ratio (A) and temperature (C) were statistically significant factors ($p < 0.001$ and $p = 0.002$, respectively), while the interaction term between A and C (AC) also showed significant influence ($p = 0.023$). In contrast, reaction time (B) was not statistically significant ($p > 0.05$), indicating a limited individual effect within the tested range.

The correlation matrix (Fig. 5B) further supported these findings: mass ratio (m_P2) showed the strongest positive correlation with fluorescence intensity ($r = 0.80$), followed by temperature ($r = 0.31$), while reaction time exhibited negligible correlation ($r = 0.13$), reaffirming its limited effect on the fluorescence outcome under the tested conditions.

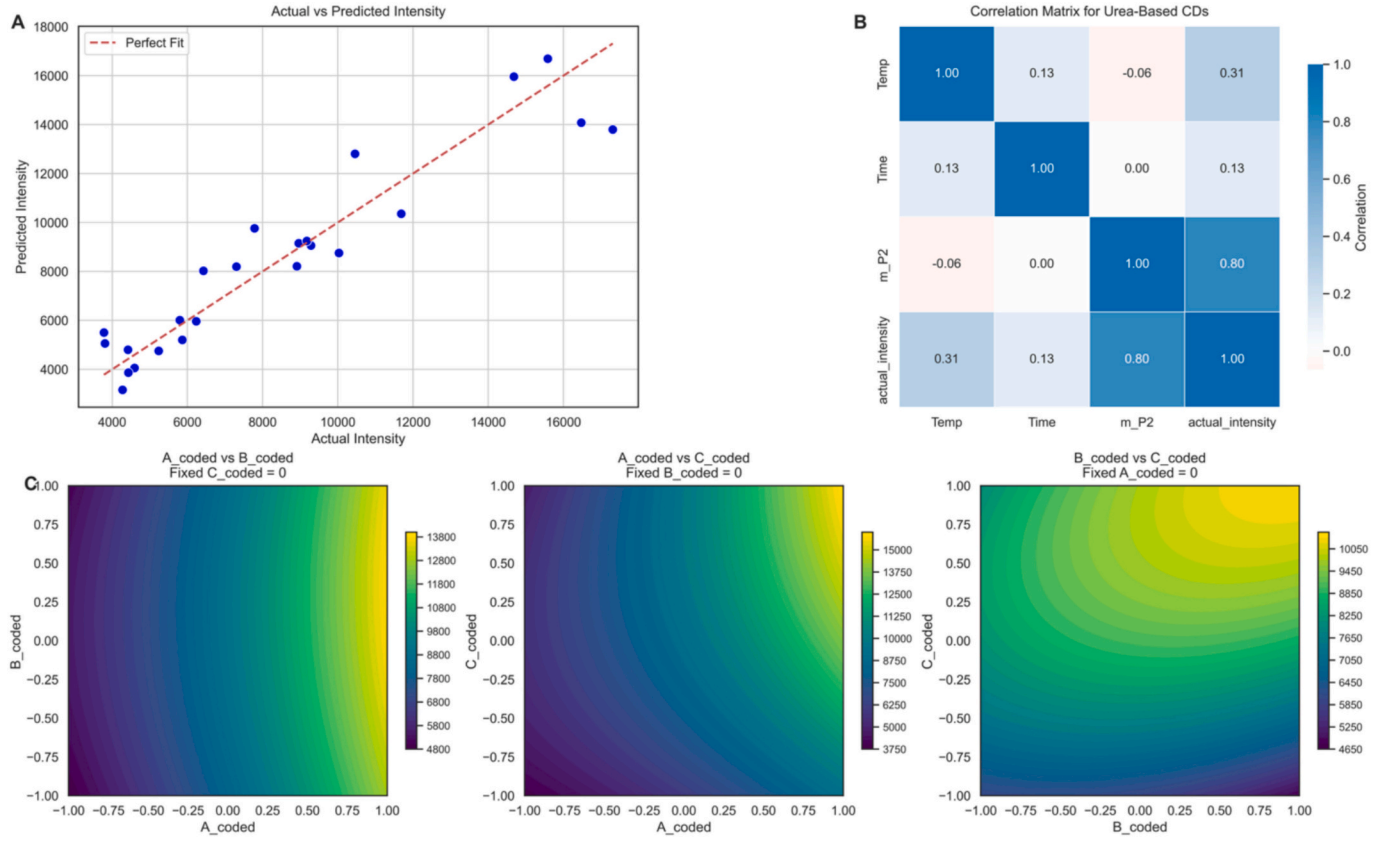

Fig. 5. Central Composite Design (CCD)-based modeling and analysis of fluorescence intensity for urea-assisted banana peel-derived carbon dots (U-BP-CDs). (**A**) Actual versus predicted fluorescence intensity of U-BP-CDs generated under different synthesis conditions, including BP:urea mass ratios (4:1, 4:2, and 4:3, *w*/w), reaction times (1, 2, and 3 h), and temperatures (160, 180, and 200 °C). (**B**) Correlation matrix of the experimental factors (mass ratio, reaction time, and temperature) and predicted fluorescence intensity. (**C**) Response surface contour plots showing the interactions among coded mass ratio (A), reaction time (B), and temperature (C) on predicted fluorescence intensity.

Contour plots (Fig. 5C) illustrated how increasing the mass ratio and pyrolysis temperature synergistically enhanced fluorescence intensity, particularly under fixed time or concentration conditions. The highest predicted intensity values were associated with the combined effects of higher urea loading and elevated temperatures.

The optimized coded conditions determined from the regression model were A_coded = +1, B_coded = +1, and C_coded = +1, corresponding to the upper limits of the design space: a 4:2 mass ratio (urea: banana peel, *w*/w), 3 h reaction time, and 200 °C pyrolysis temperature. Under these optimal conditions, the model predicted a fluorescence intensity of 16,696.06 a.u. (95% CI: 13,700.11–19,692.01 a.u.), indicating good precision of the CCD prediction.

The CCD results demonstrate that mass ratio and pyrolysis temperature were the main factors controlling fluorescence intensity, whereas reaction time had a comparatively smaller effect within the tested range. This suggests that precursor loading and thermal energy are the dominant parameters governing carbonization and nitrogen-doping efficiency during BP-CDs formation. The negligible effect of reaction time likely indicates that, within the studied range, carbonization and nitrogen incorporation had already approached a plateau, so extending the reaction time produced little additional improvement in fluorescence intensity. Similar trends have been reported in previous studies, where precursor ratio and temperature strongly influenced CD formation and fluorescence performance, while reaction time showed a diminishing effect beyond a certain threshold (Papaioannou et al., 2019; Ren et al., 2020).

The predicted optimum (A = +1, B = +1, C = +1) was located at the upper boundary of the tested design space. Thus, it should be considered the best predicted condition within the current experimental range, not a confirmed global optimum. The upper temperature limit of 200 °C was chosen based on the oven capacity, possible urea decomposition at higher temperatures, and preliminary evidence of excessive banana peel carbonization above 200 °C, which reduced fluorescence intensity. The upper limits of reaction time and precursor ratio were also based on preliminary screening. Because the response increased toward the boundary, the true optimum may lie outside the current design space. Therefore, an expanded design space and independent experimental validation of the predicted intensity (16,696.06 a.u.) are needed in future work.

3.4. Machine learning model screening

To further evaluate the predictive modeling of fluorescence intensity in the synthesis of banana peel-derived carbon dots (BP-CDs), seven machine learning (ML) algorithms were applied to the CCD dataset: Linear Regression, K-Nearest Neighbors (KNN), Support Vector Regression (SVR), Decision Tree, Random Forest, Gradient Boosting, and an Artificial Neural Network (MLPRegressor). The dataset consisted of 396 data points, with 80% used for training and 20% for testing, and 5-fold cross-validation was employed to assess model performance. The performance of each model was evaluated using two key metrics: the coefficient of determination (R^2) and root mean square error (RMSE), summarized in Table 4.

Among the models, Random Forest achieved the best performance, with the highest R^2 value (0.97), indicating the best overall predictive performance and strong ability to capture the nonlinear relationships between synthesis-related variables and fluorescence intensity. The Decision Tree model showed the lowest RMSE (516.37) and an R^2 of

Table 4
RMSE and R^2 for seven tuned machine learning models predicting fluorescence intensity of carbon dots produced from banana peel (BP-CDs).

Model	RMSE	R^2
Random Forest	542.14	0.97
Decision Tree	516.37	0.93
Gradient Boosting	879.50	0.92
K-Neighbors Regression	1073.26	0.89
Linear Regression	1965.14	0.63
Support Vector Regression	3434.76	−0.13
ANN (MLPRegressor)	4912.55	−1.88

0.93, suggesting good predictive accuracy but lower overall explanatory performance than Random Forest. Gradient Boosting also performed well, with an R^2 of 0.92 and RMSE of 879.50, followed by K-Neighbors Regression with an R^2 of 0.89 and RMSE of 1073.26.

In contrast, Linear Regression showed weaker predictive performance, with an R^2 of 0.6274 and RMSE of 1965.1415, indicating that a simple linear model was less suitable for describing the nonlinear relationships in this dataset. Support Vector Regression and ANN (MLPRegressor) performed poorly, with negative R^2 values of −0.13 and − 1.88, respectively, and high RMSE values of 3434.76 and 4912.55. These negative R^2 values indicate that these models performed worse than a simple baseline prediction based on the mean fluorescence intensity.

Overall, the tree-based models, particularly Random Forest, Decision Tree, and Gradient Boosting, outperformed the linear, distance-based, kernel-based, and neural-network models. This suggests that ensemble and tree-based approaches were better suited to capturing the complex and nonlinear effects of synthesis parameters and compositional descriptors on the fluorescence intensity of BP-CDs. Among them, Random Forest was selected as the best-performing model because it provided the highest R^2 while maintaining a low RMSE, offering a strong balance between predictive accuracy and model robustness.

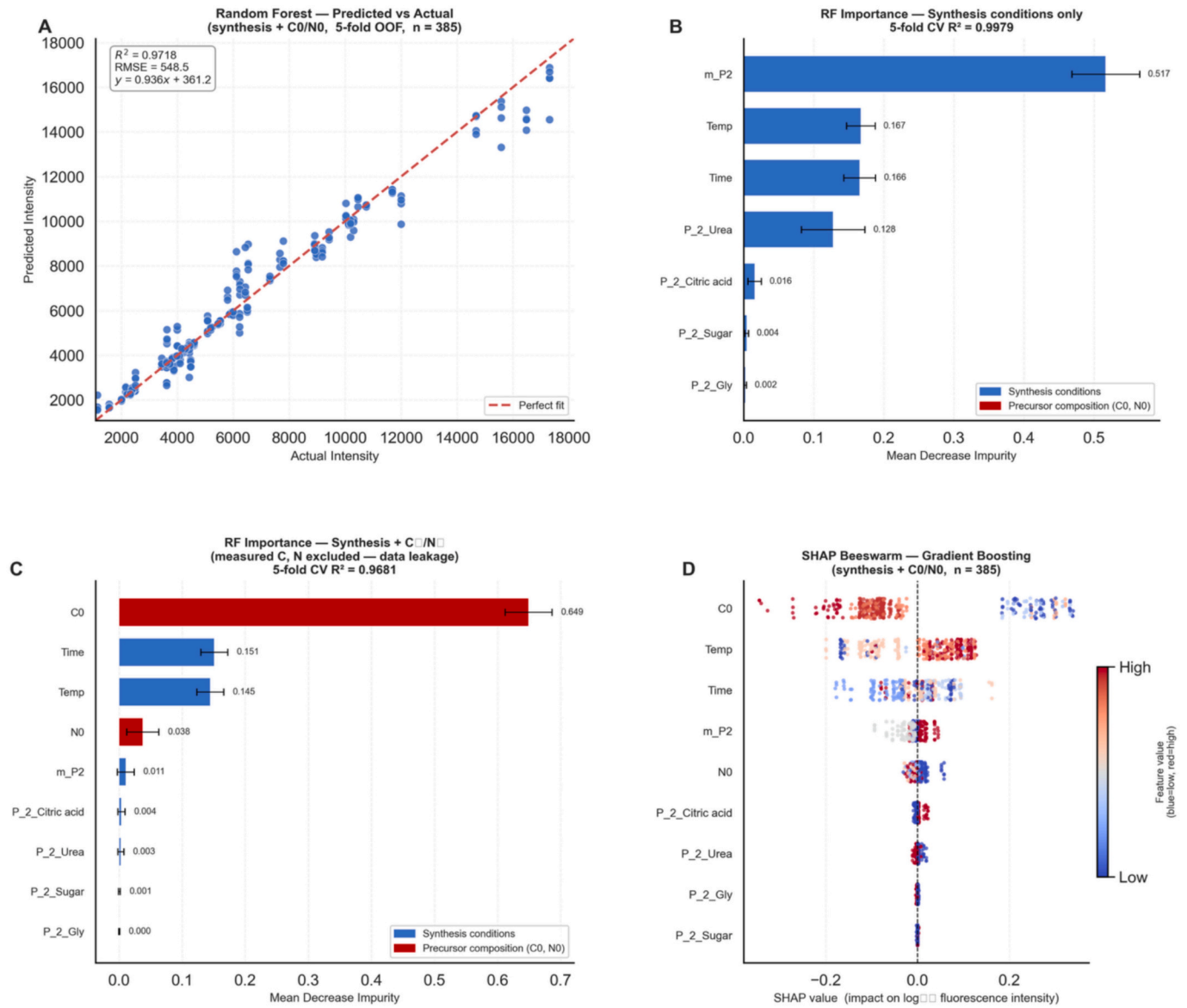

Fig. 6. Machine learning prediction and interpretability analysis of banana peel-derived carbon dots (BP-CDs) fluorescence intensity. (A) Actual versus predicted fluorescence intensity obtained using the Random Forest model with synthesis variables and measured C0/N0 descriptors under 5-fold out-of-fold cross-validation. (B) Random Forest feature importance using synthesis-condition variables only. (C) Random Forest feature importance using synthesis variables together with measured C0 and N0 descriptors. (D) SHAP beeswarm plot from the Gradient Boosting model showing the influence of synthesis variables and measured C0/N0 descriptors on predicted fluorescence intensity.

3.5. Machine learning model application

Among the seven machine learning algorithms evaluated, Random Forest showed the best overall predictive performance during model screening (Table 4). This result indicates that Random Forest was more effective than the other models in capturing the nonlinear relationships between synthesis variables and the fluorescence intensity of BP-CDs. To further evaluate model reliability and avoid over-optimistic estimation, the final prediction performance was assessed using 5-fold out-of-fold cross-validation.

Fig. 6 summarizes the performance of the Random Forest model and illustrates how the most influential experimental variables were associated with the fluorescence intensity of BP-CDs. As shown in the actual versus predicted plot using the Random Forest model with synthesis variables and measured C0/N0 descriptors (Fig. 6A), the predicted values were in good agreement with the experimental data, with most points distributed close to the identity line. The model achieved a high R^2 of 0.9718 and a low RMSE of 548.5, with the fitted regression equation $y = 0.936\times + 361.2$, confirming the strong predictive ability of the model. Some deviation was observed at higher fluorescence intensities, suggesting a slight reduction in prediction accuracy at the upper end of the response range; however, the overall trend remained well described.

To distinguish the effects of controllable synthesis conditions from post-synthesis compositional descriptors, feature importance was analyzed using two Random Forest models. When only synthesis-related variables were included (Fig. 6B), the mass ratio of precursor to banana peel-derived carbon source (m_P2) was the most influential variable, followed by pyrolysis temperature, reaction time, and the urea precursor category. This result indicates that, when elemental composition is not included in the model, fluorescence intensity is mainly governed by experimentally controllable synthesis parameters, especially precursor loading and thermal treatment conditions.

In contrast, when measured elemental descriptors were included together with synthesis variables (Fig. 6C), C0 became the dominant predictor of fluorescence intensity, accounting for the largest feature importance by a wide margin. Time and temperature remained important secondary contributors, whereas N0, m_P2, and precursor-category variables showed relatively smaller contributions. These results suggest that the fluorescence intensity of BP-CDs is strongly associated with the carbonization state of the obtained CDs, while synthesis conditions influence fluorescence both directly and indirectly through their effects on the final elemental composition.

A SHAP beeswarm analysis based on the Gradient Boosting model was further used to visualize the direction and magnitude of each feature's contribution to fluorescence prediction (Fig. 6D). C0 showed the strongest overall impact on the predicted fluorescence intensity, with higher C0 values generally contributing positively to the model output. Temperature and reaction time also showed clear effects, supporting the importance of thermal treatment in controlling fluorescence properties. In comparison, m_P2, N0, and precursor-category variables had more limited SHAP contributions, suggesting that their effects may be more dependent on interactions with carbonization and processing conditions.

Although Section 3.1 showed that urea was the most effective precursor among those tested, this does not necessarily conflict with the lower feature importance of bulk %N in the Random Forest model. The precursor-screening experiment reflects the overall effect of urea on BP-CD formation, which may involve nitrogen incorporation together with changes in carbonization behavior, surface passivation, and defect-state generation. In contrast, the ML feature importance analysis evaluates the relative predictive contribution of the measured variables across the full dataset. In this context, bulk %N may not fully represent the specific nitrogen configurations or surface chemical states that govern fluorescence, whereas %C may better reflect the extent of carbonization and conjugated structure formation. Therefore, urea may still be the most effective precursor for producing highly fluorescent BP-CDs, even though %N alone was not the dominant predictor in the ML model.

Photoluminescence in CDs is generally governed by both core-related and surface-related emissive states. The carbon core contains sp^2-hybridized domains within an oxidized amorphous carbon matrix, while surface functional groups and defect sites can also strongly influence emission behavior (Li et al., 2012; M. Liu, 2020; Zhu et al., 2013). In this study, the strong contribution of carbon content identified by the Random Forest model may indicate that the degree of carbonization plays an important role in determining fluorescence intensity. A higher carbon content may be associated with the formation of more developed sp^2 carbon domains, which can facilitate π–π^* transitions and improve radiative emission efficiency (Fu et al., 2015, p. 201; Holá et al., 2017). At the same time, changes in carbon content may reflect differences in surface oxidation and defect structures, which can affect the balance between radiative and non-radiative pathways. Therefore, the dominant predictive role of %C suggests that carbonization level and related structural features are key factors controlling the fluorescence performance of BP-CDs. However, because elemental analysis does not directly reveal the size of sp^2 domains or the nature of surface defects, further structural characterization would be required to confirm this mechanism.

The smaller contributions of %N, m_P2, and the precursor-category variables are consistent with this framework: while nitrogen doping and precursor choice are critical for initiating the formation of specific emissive species (as demonstrated by the precursor-screening experiment), the bulk fluorescence intensity of the resulting BP-CDs is governed more directly by the extent of carbonization and the maturity of the sp^2 network, both of which are captured by %C. This interpretation is also consistent with previous ML-assisted CD studies, which report that compositional and processing variables related to carbonization dominate the prediction of optical properties, while categorical precursor information often plays a secondary role once compositional descriptors are included (Chen et al., 2023; Han et al., 2020; Senanayake et al., 2022).

More broadly, the difference in variables included in the CCD and in the ML model reflects a deliberate methodological choice. The CCD was constructed using only directly controllable and experimentally feasible synthesis variables – temperature, reaction time, and m_P2 - which are appropriate for process optimization. Compositional descriptors such as %C and %N are not controllable inputs but post-synthesis measured properties of each sample; they were therefore incorporated only in the machine learning model, where they serve as descriptors of the synthesis outcome rather than as design factors. The precursor category, similarly, was handled in a separate screening step (Section 3.2) before being included in the ML feature set. This separation between controllable design factors (in CCD) and measured-outcome descriptors (in ML) explains why the two analyses include different variables and yield apparently different, yet complementary, conclusions.

Compared with the previously used Decision Tree model, Random Forest improved predictive accuracy while retaining the interpretability and robustness needed for a relatively small experimental dataset. Although more advanced approaches such as XGBoost and neural networks have achieved higher prediction accuracy in some fluorescence-related studies (Chen et al., 2023; Hong et al., 2022; Senanayake et al., 2022), Random Forest offers a practical balance between model performance and experimental interpretability. This is particularly relevant in synthesis studies, where identifying the variables governing material properties is as important as achieving high predictive accuracy.

Overall, the combined use of CCD and machine learning provided an efficient strategy for optimizing BP-CDs synthesis while also improving understanding of the variables governing fluorescence performance. The successful conversion of banana peel into highly fluorescent CDs further supports the potential of agricultural waste valorization as a sustainable approach for carbon nanomaterial production.

3.6. Stability of BP-CDs

The stability of BP-CDs in environments of varying ionic strength and pH is a critical property for their practical use in sensing and bioimaging applications. To evaluate this, two complementary stability tests were performed on a representative panel of samples covering both pre- and post-pyrolysis materials and the three precursor-derived BP-CD systems.

3.6.1. Ionic-strength (NaCl) stability

The fluorescence intensity of all five samples was measured across NaCl concentrations from 0 to 1.0 M (Fig. 7A). Urea-BP-CDs (S4) showed the highest absolute fluorescence intensity across the entire NaCl range (~825–860 a.u.) and the lowest sensitivity to ionic strength, retaining approximately 97% of their initial intensity at 1.0 M NaCl (**Fig. SI.03**). In contrast, glycine-BP-CDs (S5) showed the largest decrease (~22% loss at 1.0 M), while citric-acid-BP-CDs (S3) and the no-precursor BP-CDs (S2) lost ~17% and ~ 8%, respectively. The banana peel extract before pyrolysis (S1) showed an intermediate loss of ~15%. The greater salt sensitivity of glycine- and citric-acid-derived BP-CDs is consistent with their higher density of ionizable surface groups ($–NH_3^+$/–NH_2 and –COOH/$–COO^-$, respectively), which are more susceptible to charge screening by Na^+ and Cl^- ions under increasing ionic strength. The superior salt tolerance of urea-BP-CDs likely originates from their amide-rich, less ionizable surface chemistry combined with a more extensively carbonized core.

3.6.2. pH stability

The fluorescence response of all five samples was evaluated across pH 3, 5, 7, 9, and 11 (Fig. 7B). When normalised to pH 7, urea-BP-CDs (S4) again demonstrated remarkable stability, with relative intensity varying between 98% and 104% across the entire pH range (**Fig. SI.04**). Citric-acid-BP-CDs (S3) showed a modest bell-shaped response with maximum emission around pH 7–9 (93–101%), consistent with the partial deprotonation of surface carboxyl groups in this pH window. The banana peel extract before pyrolysis (S1) and the no-precursor BP-CDs (S2) showed comparable behavior, with peak emission at pH 7 and gradual decreases toward alkaline pH (down to ~75% and ~ 88%, respectively at pH 11), likely reflecting alkaline-induced quenching of native or partially-carbonized fluorophores. In contrast, glycine-BP-CDs (S5) exhibited pronounced pH sensitivity, with relative intensity dropping to ~80% at acidic pH and rising to ~119% at pH 11. This behavior is attributed to the deprotonation of amino groups ($–NH_3^+$ → $–NH_2$) on the CD surface, which alters the electronic structure of the surface emissive states and reduces non-radiative photoinduced electron-transfer quenching, in agreement with prior reports on amino-rich CDs.

Taken together, the dual ionic-strength and pH stability tests identify urea-BP-CDs (S4) as uniquely robust among the tested samples, exhibiting both the highest absolute fluorescence intensity and the lowest sensitivity to environmental ionic conditions. This combination makes urea-BP-CDs particularly suitable for fluorescence-based detection in complex aqueous matrices, including biological fluids, food extracts, and environmental waters, where ionic strength and pH can vary considerably. Additional stability assessments (photostability and long-term storage stability), which are essential for full validation of practical sensing performance, were not addressed in the present study and are identified as priorities for our immediate follow-up work.

4. Future perspectives

Given their strong fluorescence, relatively high quantum yield, and low-cost biomass-derived origin, the optimized banana peel-derived carbon dots (BP-CDs) show promising potential for several immediate applications. Their stable blue emission makes them attractive candidates for fluorescent sensing platforms, particularly for metal ion detection and other environmental or food-related analytes. In addition, their simple and energy-efficient preparation suggests potential for scalable production of sustainable fluorescent nanomaterials. With further evaluation of selectivity, sensitivity, and matrix effects, these BP-CDs could be explored for practical sensing applications. Moreover, after appropriate biocompatibility and toxicity assessment, the optimized BP-CDs may also have potential in bioimaging and related biomedical fields. These application prospects further highlight the translational value of converting banana peel waste into functional carbon-based nanomaterials. In addition, detailed characterization of nitrogen speciation in the optimized BP-CDs, for example by X-ray photoelectron spectroscopy (XPS) and solid-state NMR, will be carried out to clarify the relative contributions of pyrrolic, pyridinic, graphitic, and amino nitrogen configurations to the observed fluorescence enhancement.

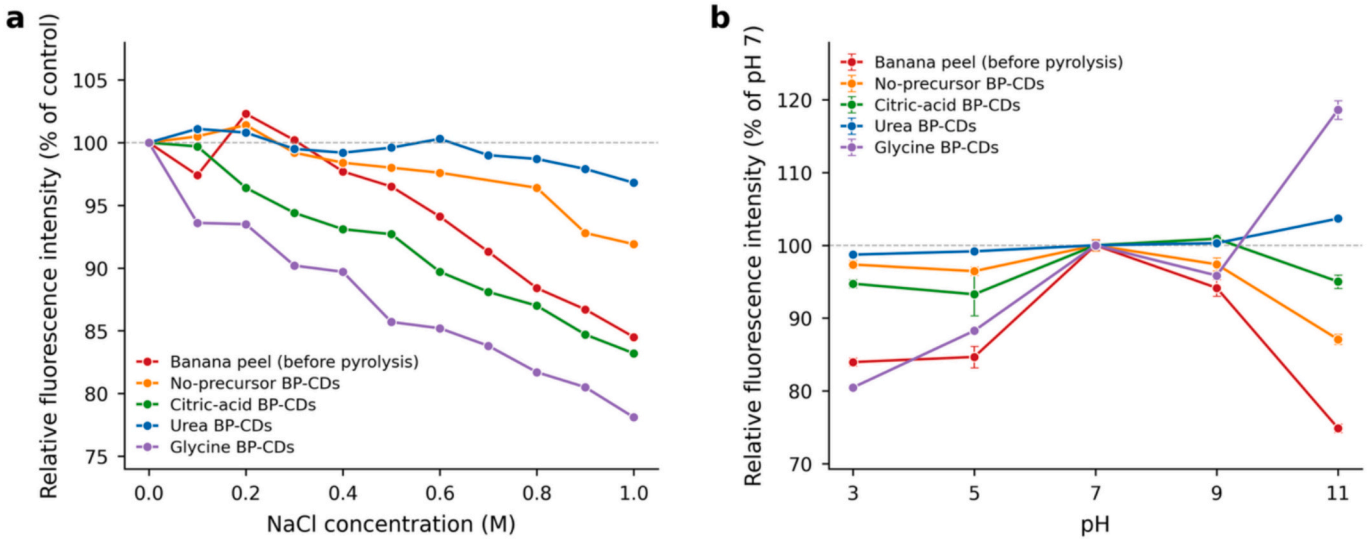

Fig. 7. Ionic-strength and pH stability of banana peel-derived carbon dots (BP-CDs). **(A)** Relative fluorescence intensity (normalised to the 0 M control, %) of five samples in NaCl solutions (0–1.0 M): banana peel extract before pyrolysis (S1), no-precursor BP-CDs (S2), citric-acid BP-CDs (S3), urea BP-CDs (S4), and glycine BP-CDs (S5). The dashed line indicates the 100% reference. **(B)** Relative fluorescence intensity (normalised to the pH 7.0 control, %) of five samples at pH 3, 5, 7, 9, and 11 in Britton–Robinson buffer. Letters above each bar denote statistically homogeneous groups within the same sample (Duncan's multiple-range test, $p < 0.05$). All measurements were carried out at λ_ex = 360 nm, corrected for an 8-fold dilution factor, and reported as mean ± SD of three independent replicates ($n = 3$).

5. Conclusion

This study demonstrates that banana peel can be valorized into highly fluorescent carbon dots through a simple low-temperature pyrolysis approach. Among the tested precursors, urea was the most effective for enhancing fluorescence performance, and the optimized synthesis conditions were a 4:2 urea-to-banana peel mass ratio, 3 h reaction time, and 200 °C pyrolysis temperature. Under these conditions, the obtained CDs showed high fluorescence intensity and a quantum yield of approximately 40%. Both the experimental results and machine learning analysis confirmed that carbon content and thermal processing conditions were the main factors influencing fluorescence performance.

These findings support the potential of banana peel as a low-cost and sustainable precursor for CDs production. Future work should focus on improving control over particle structure and surface chemistry, validating the synthesis strategy on a larger scale, and exploring practical applications in food analysis, sensing, bioimaging, and optoelectronic materials. Further studies on stability, reproducibility, and application-specific performance will also be important to support real-world use of these biomass-derived carbon dots.

CRediT authorship contribution statement

Duyen H.H. Nguyen: Writing – original draft, Visualization, Methodology, Formal analysis, Conceptualization. **József Prokisch:** Writing – review & editing, Validation, Supervision, Resources, Project administration, Funding acquisition.

Declaration of competing interest

The authors declare that they have no known competing financial interests or personal relationships that could have appeared to influence the work reported in this paper.

Acknowledgements

Supported by the University of Debrecen Scientific Research Bridging Fund (DETKA). Supported by the University of Debrecen Program for Scientific Publication.

Appendix A. Supplementary data

Supplementary data to this article can be found online at https://doi.org/10.1016/j.foodchem.2026.149840.

Data availability

Data will be made available on request.

References

Bosu, S., Rajamohan, N., Sagadevan, S., & Raut, N. (2023). Biomass derived green carbon dots for sensing applications of effective detection of metallic contaminants in the environment. *Chemosphere, 345*, Article 140471. https://doi.org/10.1016/j.chemosphere.2023.140471

Boyle, O., Xiao, B., & Mangwandi, C. (2025). Valorization of Banana Peel waste into advanced adsorbent beads for the removal of emerging pollutants from wastewater. *Materials, 18*(5), 1084. https://doi.org/10.3390/ma18051084

Chakravarthi, M. A., Sharma, S., Sahu, A., Murthy, T. S. A. T., & Jain, S. (2024). Machine learning algorithms for automated synthesis of biocompatible nanomaterials. *International Conference on Intelligent Systems and Advanced Applications (ICISAA), 2024*, 1–6. https://doi.org/10.1109/ICISAA62385.2024.10829264

Chen, J., Zhang, M., Xu, Z., Ma, R., & Shi, Q. (2023). Machine-learning analysis to predict the fluorescence quantum yield of carbon quantum dots in biochar. *Science of the Total Environment, 896*, Article 165136. https://doi.org/10.1016/j.scitotenv.2023.165136

De, B., & Karak, N. (2013). A green and facile approach for the synthesis of water soluble fluorescent carbon dots from banana juice. *RSC Advances, 3*(22), Article 8286. https://doi.org/10.1039/c3ra00088e

Diao, S., Wu, Q., Li, S., Xu, G., Ren, X., Tan, L., Jiang, G., Song, P., & Meng, X. (2025). From synthesis to properties: Expanding the horizons of machine learning in nanomaterials research. *Materials Horizons, 12*(12), 4133–4164. https://doi.org/10.1039/D4MH01909A

Fu, M., Ehrat, F., Wang, Y., Milowska, K. Z., Reckmeier, C., Rogach, A. L., … Feldmann, J. (2015). Carbon dots: A unique fluorescent cocktail of polycyclic aromatic hydrocarbons. *Nano Letters, 15*(9), 6030–6035. https://doi.org/10.1021/acs.nanolett.5b02215

Gao, T., Huang, H., & Liu, Y. (2025). Machine learning-driven nanoscale synthesis for Electrocatalytic performance: From data-driven methodologies to closed-loop optimization. *Advanced Materials, e08263*. https://doi.org/10.1002/adma.202508263

Gilman, J., Walls, L., Bandiera, L., & Menolascina, F. (2021). Statistical Design of Experiments for synthetic biology. *ACS Synthetic Biology, 10*(1), 1–18. https://doi.org/10.1021/acssynbio.0c00385

Han, Y., Tang, B., Wang, L., Bao, H., Lu, Y., Guan, C., … Wu, M. (2020). Machine-learning-driven synthesis of carbon dots with enhanced quantum yields. *ACS Nano, 14*(11), 14761–14768. https://doi.org/10.1021/acsnano.0c01899

Hoan, B. T., Tam, P. D., & Pham, V.-H. (2019). Green synthesis of highly luminescent carbon quantum dots from lemon juice. *Journal of Nanotechnology, 2019*, 1–9. https://doi.org/10.1155/2019/2852816

Holá, K., Sudolská, M., Kalytchuk, S., Nachtigallová, D., Rogach, A. L., Otyepka, M., & Zboril, R. (2017). Graphitic nitrogen triggers red fluorescence in carbon dots. *ACS Nano, 11*(12), 12402–12410. https://doi.org/10.1021/acsnano.7b06399

Hong, Q., Wang, X.-Y., Gao, Y.-T., Lv, J., Chen, B.-B., Li, D.-W., & Qian, R.-C. (2022). Customized carbon dots with predictable optical properties synthesized at room temperature guided by machine learning. *Chemistry of Materials, 34*(3), 998–1009. https://doi.org/10.1021/acs.chemmater.1c03220

Hui, Y. Y., Chang, H., Dong, H., & Zhang, X. (Eds.). (2019). *Carbon nanomaterials for bioimaging, bioanalysis, and therapy* (1st ed.). Wiley. https://doi.org/10.1002/9781119373476.

Hundekari, D. S., Prakash, D. J., Choudari, S., & 4Md Asaduzzaman, 5Bijoy Laxmi Koley, 6Anupam Kumar Biswas, & Samujjwal Ray.. (2024). Machine learning-driven nanomaterial design: Predictive modeling for enhanced performance in electronics. *Nanotechnology Perceptions, 2039–2051*. https://doi.org/10.62441/nano-ntp.vi.3066

Jamaludin, N., Rashid, S. A., & Tan, T. (2019). Natural biomass as carbon sources for the synthesis of Photoluminescent carbon dots. In *Synthesis, technology and applications of carbon nanomaterials* (pp. 109–134). Elsevier. https://doi.org/10.1016/B978-0-12-815757-2.00005-X.

Jones, S. S., Sahatiya, P., & Badhulika, S. (2017). One step, high yield synthesis of amphiphilic carbon quantum dots derived from chia seeds: A solvatochromic study. *New Journal of Chemistry, 41*(21), 13130–13139. https://doi.org/10.1039/C7NJ03513F

Kabenge, I., Omulo, G., Banadda, N., Seay, J., Zziwa, A., & Kiggundu, N. (2018). Characterization of Banana peels wastes as potential slow pyrolysis feedstock. *Journal of Sustainable Development, 11*(2), 14. https://doi.org/10.5539/jsd.v11n2p14

Kostromin, S., Borodina, A., Podshivalov, A., Pankin, D., Zhigalina, O., & Bronnikov, S. (2023). Characterization of carbon quantum dots obtained through citric acid pyrolysis. *Fullerenes, Nanotubes, and Carbon Nanostructures, 31*(10), 931–939. https://doi.org/10.1080/1536383X.2023.2224467

Li, H., Kang, Z., Liu, Y., & Lee, S.-T. (2012). Carbon nanodots: Synthesis, properties and applications. *Journal of Materials Chemistry, 22*(46), 24230. https://doi.org/10.1039/c2jm34690g

Liu, M. (2020). Optical properties of carbon dots: A review. *Nanoarchitectonics, 1*(1), 1–12. https://doi.org/10.37256/nat.112020124.1-12

Liu, W., Xu, S., Liang, R., Wei, M., Evans, D. G., & Duan, X. (2017). In situ synthesis of nitrogen-doped carbon dots in the interlayer region of a layered double hydroxide with tunable quantum yield. *Journal of Materials Chemistry C, 5*(14), 3536–3541. https://doi.org/10.1039/C6TC05463C

Liu, Y., Tang, Y., Xu, Q., Cao, Y., Wei, J., Liang, Z., Jiang, X., Wu, Y., & Guo, C. (2024). Solvothermal regulation of fluorescence quantum yield of carbon dots derived from biomass for zebrafish imaging. *Journal of Luminescence, 271*, Article 120583. https://doi.org/10.1016/j.jlumin.2024.120583

Liu, Y., Yong, C., Tong, B., Li, Y., Wang, N., & Lei, Y. (2022). Modification of carbon dots derived from biomass by exogenous nitrogen doping: Action mechanism and difference analysis. *Optical Materials, 134*, Article 113144. https://doi.org/10.1016/j.optmat.2022.113144

Nguyen, D., El-Ramady, H., & Prokisch, J. (2024). Food safety aspects of carbon dots: A review. *Environmental Chemistry Letters*. https://doi.org/10.1007/s10311-024-01779-3

Nguyen, D., Muthu, A., El-Ramady, H., Daróczi, L., Nagy, L., Kéki, S., … Prokisch, J. (2024). *Optimization of extraction conditions to synthesize green carbon nanodots using the Maillard reaction. Materials advances, 10.1039.D4MA00037D*. https://doi.org/10.1039/D4MA00037D

Nguyen, D. H. H., Muthu, A., Elsakhawy, T., Sheta, M. H., Abdalla, N., El-Ramady, H., & Prokisch, J. (2025). Carbon nanodots-based sensors: A promising tool for detecting and monitoring toxic compounds. *Nanomaterials, 15*(10), Article 725. https://doi.org/10.3390/nano15100725

Ogi, T., Aishima, K., Permatasari, F. A., Iskandar, F., Tanabe, E., & Okuyama, K. (2016). Kinetics of nitrogen-doped carbon dot formation via hydrothermal synthesis. *New Journal of Chemistry, 40*(6), 5555–5561. https://doi.org/10.1039/C6NJ00009F

Papaioannou, N., Titirici, M.-M., & Sapelkin, A. (2019). Investigating the effect of reaction time on carbon dot formation, structure, and optical properties. *ACS Omega, 4*(26), 21658–21665. https://doi.org/10.1021/acsomega.9b01798

Prado, M. B., Truong, N. T., & Wanekaya, A. K. (2023). Improving the quantum yield of nitrogen-doped carbon dots by varying dopant ratios and pH. *Sensors and Actuators Reports, 6*, Article 100165. https://doi.org/10.1016/j.snr.2023.100165

Prokisch, J., Nguyen, D. H. H., Muthu, A., Posta, J., & Béni, A. (2026). Quantitative determination of carbon nanodots in processed foods using HPLC-SEC with fluorescence detection. *Microchemical Journal, 224*, Article 117773. https://doi.org/10.1016/j.microc.2026.117773

Quaid, T., Ghalandari, V., & Reza, T. (2022). Effect of synthesis process, synthesis temperature, and reaction time on chemical, morphological, and quantum properties of carbon dots derived from loblolly pine. *Biomass, 2*(4), 250–263. https://doi.org/10.3390/biomass2040017

Ren, J., Malfatti, L., & Innocenzi, P. (2020). Citric acid derived carbon dots, the challenge of understanding the synthesis-structure relationship. *C, 7*(1), 2. https://doi.org/10.3390/c7010002

Santos, N., Santana, P. A., Osorio-Roman, I., Jara-Gutiérrez, C., Villena, J., & Ahumada, M. (2025). Effect of temperature on the carbonization process of cationic carbon dots: A physicochemical and in vitro study. *RSC Advances, 15*(16), 12814–12824. https://doi.org/10.1039/D5RA00062A

Senanayake, R. D., Yao, X., Froehlich, C. E., Cahill, M. S., Sheldon, T. R., McIntire, M., … Hernandez, R. (2022). Machine learning-assisted carbon dot synthesis: Prediction of emission color and wavelength. *Journal of Chemical Information and Modeling, 62*(23), 5918–5928. https://doi.org/10.1021/acs.jcim.2c01007

Stan, C. S., Albu, C., Coroaba, A., Popa, M., & Sutiman, D. (2015). One step synthesis of fluorescent carbon dots through pyrolysis of N-hydroxysuccinimide. *Journal of Materials Chemistry C, 3*(4), 789–795. https://doi.org/10.1039/C4TC02382J

Wang, J., Zhang, P., Huang, C., Liu, G., Leung, K. C.-F., & Wáng, Y. X. J. (2015). High performance Photoluminescent carbon dots for in vitro and in vivo bioimaging: Effect of nitrogen doping ratios. *Langmuir, 31*(29), 8063–8073. https://doi.org/10.1021/acs.langmuir.5b01875

Wang, L., Yin, Y., Jain, A., & Zhou, H. S. (2014). Aqueous phase synthesis of highly luminescent, nitrogen-doped carbon dots and their application as bioimaging agents. *Langmuir, 30*(47), 14270–14275. https://doi.org/10.1021/la5031813

Xu, X., Ray, R., Gu, Y., Ploehn, H. J., Gearheart, L., Raker, K., & Scrivens, W. A. (2004). Electrophoretic analysis and purification of fluorescent single-walled carbon nanotube fragments. *Journal of the American Chemical Society, 126*(40), 12736–12737. https://doi.org/10.1021/ja040082h

Yasin, M., Gangan, S., & Panchal, S. K. (2025). Banana peels: A genuine waste or a wonderful opportunity? *Applied Sciences, 15*(6), 3195. https://doi.org/10.3390/app15063195

Yorozuya, H., Ashrafi, N. E., Sato, K., Islam, A., Fukae, R., Tagashira, Y., & Iimori, T. (2025). Synthesis and fluorescence mechanism of nitrogen-doped carbon dots utilizing biopolymer and urea. *Molecules, 30*(9), 2068. https://doi.org/10.3390/molecules30092068

Zattar, A. P. P., Fajardo, G. L., De Mesquita, J. P., & Pereira, F. V. (2021). Luminescent carbon dots obtained from chitosan: A comparison between different methods to enhance the quantum yield. *Fullerenes, Nanotubes, and Carbon Nanostructures, 29*(6), 414–422. https://doi.org/10.1080/1536383X.2020.1854742

Zhu, S., Meng, Q., Wang, L., Zhang, J., Song, Y., Jin, H., … Yang, B. (2013). Highly Photoluminescent carbon dots for multicolor patterning, sensors, and bioimaging. *Angewandte Chemie International Edition, 52*(14), 3953–3957. https://doi.org/10.1002/anie.201300519